PERGAMON

International Journal of Multiphase Flow 27 (2001) 1487–1516

International Journal of Multiphase Flow

www.elsevier.com/locate/ijmulflow

Explosive vaporization of superheated liquids by boiling fronts

P. Reinke, G. Yadigaroglu *

Institute of Energy Technology, Swiss Federal Institute of Technology, ETH-Zentrum – CLT, CH-8092 Zurich, Switzerland

Received 18 May 2000; received in revised form 23 March 2001

Abstract

Up to 2 l of metastable propane, butane, refrigerant R-134a and water were released from glass receptacles without nucleation sites and expanded to atmospheric pressure over a range of initial superheats created by the sudden depressurization. Above a certain superheat threshold, vaporization occurred only in a thin surface zone of intense boiling and liquid fragmentation. This boiling front traveled from the free surface into the bulk of the superheated liquid and ejected a high-velocity vapor/liquid stream. For pipe sizes in the range from 14 to 80 mm, no significant influence of the cross-sectional area on the front velocity was noted. The complex interaction of vaporization and fragmentation of the superheated liquid at the boiling front appeared as a self-amplifying process, as also noted by others. Below a certain superheat threshold, there was no front propagation, and the vaporization could not carry away surplus liquid. The two-phase flow created at the boiling front had a velocity significantly lower than that expected from isentropic phase change. The pressure created by the acceleration of the two-phase mixture reduces the superheat in the liquid and attenuates the phenomena, as experiments with orifices have shown. An extensive non-dimensional analysis of the data was conducted. The threshold for boiling front creation and the front velocity were correlated in terms of the relevant thermophysical properties and the superheat; the data of other investigators agreed well with the proposed new correlations.

Keywords: Explosive boiling; Explosive vaporization; Sudden depressurization; Superheated liquid; Depressurization superheated liquid; Boiling front; Rapid nucleation; Interfacial instabilities

* Corresponding author. Tel.: +41-1-632-4615; fax: +41-1-632-1166.
E-mail address: yadi@iet.mavt.ethz.ch (G. Yadigaroglu).

0301-9322/01/$ - see front matter
PII: S0301-9322(01)00023-4

1. Introduction

This study focuses on the explosive vaporization of superheated liquids. Superheating occurs by the sudden depressurization of the liquid. The work was motivated by the need to understand the influence of such a phase transition on the catastrophic failure of pressure vessels filled with liquefied gas.

Several approaches have been used to predict the behavior of superheated liquids. A number of small-scale experiments mostly attempted to determine the onset of homogeneous nucleation. The explosive vaporization of single drops was investigated by Moore (1956), Jarvis et al. (1975), Blander and Katz (1975), Shepherd and Sturtevant (1982), Frost and Sturtevant (1986), Yang and Maa (1987), Nguyen et al. (1988), Frost (1988) and McCann et al. (1989). In the absence of nucleation sites, the liquid superheat could approach the temperature of homogeneous nucleation.

Other experiments focused on the behavior of liquid at superheats lower than the ones leading to homogeneous nucleation and for volumes larger than those of single drops. Grolmes and Fauske (1974) performed the first experiments on vaporization with completely suppressed bulk and wall nucleation; they released fluids from a glass pipe and observed a "boiling front" originating at the free liquid surface and propagating into the stagnant superheated liquid. Wall and bulk nucleation was prevented by intensive cleaning, rinsing of the test section and/or by degassing and extensive prior boiling of the test fluid. Peterson et al. (1984) and Das et al. (1987) conducted similar experiments and noted significantly higher mass transfer rates than for quiet evaporation alone. In the work of Hill (1991), Hill and Sturtevant (1990) and Sugioka (1991), boiling fronts are examined more extensively. The qualitative features of a boiling front are described and measurements of quantities such as front velocity, pressures, and the properties of the two-phase stream that is generated are given. However, the number of fluids utilized, the number of data points and the range of superheats were limited. Similar experiments with and without nucleation on walls were conducted by Barbone et al. (1995).

The purpose of the work presented in this paper was to fill some gaps in the current knowledge on the propagation of boiling fronts and extend the available database with numerous new, carefully conducted experiments. Several liquids were released to atmospheric pressure over a range of superheats not covered by previous experiments. The superheats reached in the present experiments are below those needed for homogeneous nucleation.

The various fluids used covered a wide range of properties, allowing investigation of individual property effects. The experiments were designed to eliminate nucleation on the walls; thus, the propagation of boiling fronts at the free surface of superheated fluids could be studied. Using the experimental database, the influence of various parameters was evaluated and correlations describing the threshold superheat for front propagation and the vaporization rate (front velocity) were developed; their predictions were also compared to data of other investigators.

2. Experimental setup

Propane, *n*-butane, refrigerant R-134a and water were selected as the test substances because of their sufficiently different physical properties and/or their technical importance. In contrast to other previous experiments, the substances were released to atmospheric pressure in order to

obtain findings of industrial relevance. The superheat was varied by changing the initial fluid temperature T_{in}. The release conditions determined the *nominal* superheat ΔT_{nom} of the fluid

$$\Delta T_{nom} = T_{in} - T_{sat}(p_{1\ bar}), \tag{1}$$

where $T_{sat}(p_{1\ bar})$ is the saturation temperature of the fluid at 1 bar (roughly atmospheric) pressure.

Due to acceleration of the fluid and friction, the pressure at the boiling front was higher than atmospheric, and this resulted in a lower *real* superheat ΔT_{real} prevailing in the stagnant superheated liquid at the front and behind the front

$$\Delta T_{non} > \Delta T_{real} = T_{in} - T_{sat}(p_{fr}), \tag{2}$$

where $T_{sat}(p_{fr})$ is the saturation temperature at the pressure prevailing at or behind the boiling front.

The range of superheats covered by the experiments was limited for technical and safety reasons. A maximum value was reached with butane at a nominal superheat of 73 K. This is, however, still about 32 K below the temperature of homogeneous nucleation (Blander and Katz, 1975) and is the highest superheat achieved in investigations of boiling fronts so far.

The major part of the experimental work was performed in a setup that produced upward releases from a vertical glass pipe with downward propagation of the boiling front. Another device allowed the opening of a circumferential cross-section between two parallel glass plates. This resulted in a full 360° radial outflow from a flat cylindrical vessel and allowed observations of boiling fronts advancing radially from the surface to the center of the volume of superheated liquid. Reinke (1996) describes details of this second set of experiments, as well as the safety precautions necessary for conducting this potentially hazardous work.

2.1. Releases from a glass pipe

The experimental setup shown in Fig. 1 was designed to:

- permit sudden depressurization to ambient pressure, that is, complete opening of the test section in a millisecond time scale,
- avoid nucleation sites within the test fluid that could influence the boiling front,
- allow investigations with propane, butane, water and R-134a in a range of pressures from 1 to 10 bar, corresponding to saturation temperatures from −42°C to 150°C,
- allow recordings on film, as well as pressure and temperature measurements,
- permit use of differently sized test sections.

The central part of the setup, Fig. 1, was occupied by interchangeable glass pipes (GP) having a length of 500 mm, with inner diameters up to 80 mm. These were made of borosilicate glass and were surrounded by a temperature-conditioning jacket (TCJ) of rectangular cross-section made of heat-resistant glass. The jacket was filled with a transparent heat transfer agent (water, glycol/water mixture, or silicone oil, depending on the temperature) and permitted filming of the central pipe without major optical distortion. A thermostat (Haake DC3-K15) established a homogeneous temperature in the pipe, in the range −15 to 150°C. For experiments at initial temperatures below the dew point of the ambient air, the observation glasses at the bottom and the sides of the box were enclosed in thin chambers made of acrylic glass; a small flow of

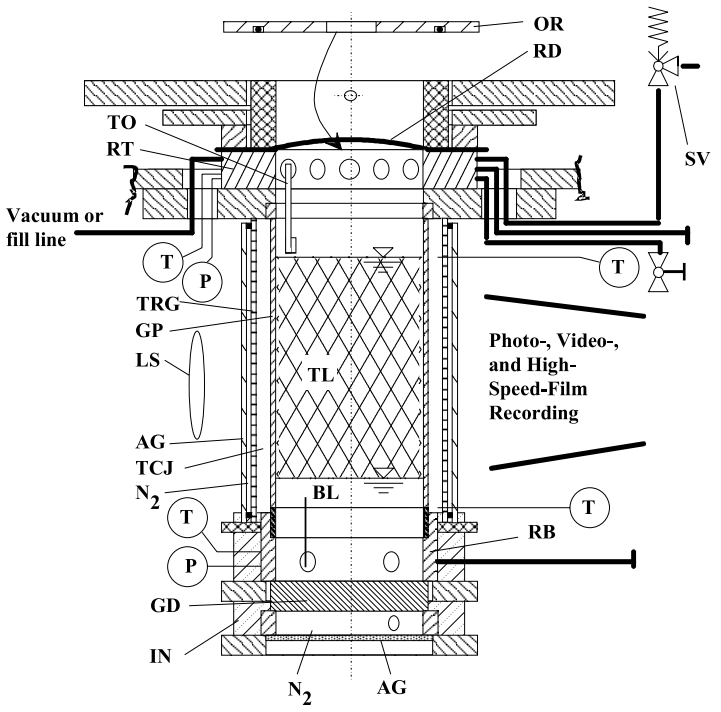

Fig. 1. Experimental setup for releasing superheated liquid from pipe. (AG: Acrylic glass; BL: Buffer liquid; GD: Glass disk; GP: Glass pipe; IN: Insulation; LS: Light source; N_2: Nitrogen; OR: Orifice; P: Pressure measurement; RB: Bottom ring; RD: Rupture disk; RT: Top ring; SV: Safety valve; T: Temperature measurement; TCJ: Temperature-conditioning jacket; TL: Test liquid; TO: Top outlet; TRG: Temperature-resistant glass).

nitrogen gas through these spaces prevented condensation of ambient humidity on the observation glasses.

The flat ends of the glass pipes were fixed between an arrangement of rings and flanges consisting either of stainless steel or aluminum. The rings at the top (RT) and the bottom (RB) allowed penetrations by instrumentation and various line connections to the glass pipes. The bottom of the test volume was closed by a glass disk (GD) which permitted observations in the direction of the pipe axis. A rupture disk (RD) closed the top of the pipe. This disk could be opened by a new type of mechanism that produced a "clean," obstruction-free flow area. This mechanism exploited the fact that a small enlargement of the diameter of a circular flange leads to a major increase in tension of the rupture sheet. Instead of expensive commercial RDs, ordinary foil made of sheet metal could be used. The patented mechanism (Reinke, 1995) is described in more detail by Reinke (1996, 1997b).

In combination with procedures for cleaning, vacuuming and filling the test section with test fluid, the equipment allowed use of a new method for eliminating nucleation sites. The essential steps of this novel technique consisted of:

- emptying all cavities by vacuuming,
- filling the cavities with a buffer liquid that fills up temporarily the test volume completely,

- introducing and pressurizing the test fluid and simultaneously removing the buffer liquid without exposing the walls of the test section to a gas atmosphere.

The method, as well as its various modifications necessary for fluids with different thermophysical properties, is presented in more detail by Reinke (1997a). In general, the test liquid was introduced and condensed directly into the pipe and was afterwards slightly pressurized by nitrogen. The nitrogen pressure was applied for a short time interval (about 10 min) for the test fluid temperature to reach that of the surrounding conditioning liquid.

The largest pipe diameter of 80 mm allowed other equipment to be placed inside the test pipe. The following items were used, depending on the objectives of certain investigations:

- A *glass funnel* provided a test section with continuously decreasing cross-sectional area. This geometry was used to investigate the influence of cross-sectional area on the velocity of the boiling front. The cross-sectional area of the funnel at the bottom was approximately 1/50th of the value at the top ($d_{top} = 70$ mm, $d_{bottom} = 10$ mm, height = 150 mm).
- A *flattened pipe* (rectangular cross-section in the field of view: ca. 60×4 mm, height: 100 mm) and a *small, non-pressure-resistant glass pipe* ($d = 14$ mm) were installed inside the pipe to get a better view of the internal structure of the boiling front.

In addition to the above, an *orifice* (OR) with an opening of 30 mm could be mounted directly below the RD. It allowed investigation of the effect of elevated pressures downstream of the boiling front. A *2-m-long acrylic glass pipe* of 80-mm internal diameter could also be placed on top of the RD to measure the velocity of droplets at different distances from the vaporization zone. In general, these modifications were used for a limited number of runs only.

2.2. Measuring methods and data acquisition

The test fluid was depressurized and released from an initially almost saturated state by opening the RD. A high-speed Hycam camera (max. 8000 frames/s) and/or a video camera (CCD-Panasonic NV MS 95 E, 50 frames/s, 1/16 000 s exposure time) recorded the boiling process. A spotlight with a 2500-W quartz bulb served as the illumination source. Two transducers were used to measure the pressure in the test section (Kistler 603b, piezoelectric, natural frequency 400 kHz, 0–200 bar; Kulite XCQ-062-17A, piezoresistive, natural frequency 1600 kHz, 0–17 bar; both calibrated to an accuracy of about 2% of the measured value). Their signals were sent to a digital storage oscilloscope (LeCroy 9314M). Chromel–Alumel, K-type thermocouples (with a calibrated accuracy better than 0.5 K) were installed at the bottom and at the exit of the pipe. These were used only to determine the temperature of the buffer liquid *prior* to release; any solid transducer placed into the metastable liquid would have served as an artificial nucleation site. The temperatures of the vapor space above the test liquid, of the conditioning liquid, and of the ambient air were also measured.

In a few experiments, liquid propane was colored prior to release and the expelled jet was directed onto a rotating disk covered with paper. The impact diameter of the stained droplets impinging on paper allowed their diameters before impingement to be determined. The original droplet sizes could be inferred from the spots on the paper using a predetermined spreading correction factor (Reinke, 1996).

3. Qualitative features of the boiling fronts

Since nucleation from sites on the test section wall could be avoided, vaporization of the superheated liquid occurred only on its free surface. No bulk nucleation was observed. The vaporization zone, i.e., the boiling front, propagated into the bulk of the superheated liquid. The investigation was focused upon the following: mechanism of front propagation; influence of superheat, geometry and properties of the fluid on propagation velocity; two-phase flow velocity and pressure increase at the boiling front due to acceleration of the fluid; effect of increased pressure (orificing) on the boiling front.

In agreement with previous observations by Hill and Sturtevant (1990), a transient start-up period, followed by a period of quasi-steady boiling front propagation was noted. Steady front propagation observations were similar to those made by these authors. Since most of the liquid is released during the quasi-steady boiling front propagation, this investigation focused on this period.

3.1. Global view of the boiling front

After opening the test section and suddenly depressurizing the test liquid, a phase-change front traveling violently into the superheated liquid became visible. The boiling zone exhibited intense vaporization and fine-scale fragmentation. A high-velocity *two-phase* flow region was produced downstream of the front, since the latent heat could not vaporize *all* the liquid. The example of Fig. 2 showing three video frames from a release of superheated butane illustrates this situation. Similar results were obtained using propane, R-134a and water.

On the first frame of Fig. 2, the pipe is closed and the liquid and vapor are in a saturated or slightly sub-cooled state. The remaining buffer liquid, in this case water, can be seen below the test fluid. After opening and depressurizing the glass pipe, the following two frames show the propagation of the boiling front into the now superheated butane. The contour of the phase boundary changed continuously during propagation. Tips of the front sped forward while other areas

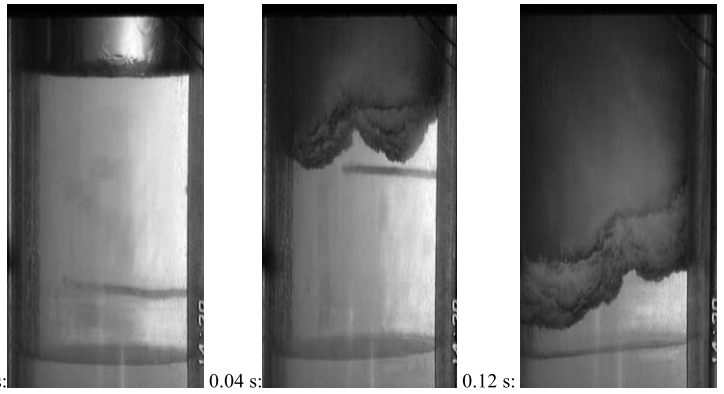

Fig. 2. Propagation of a boiling front (advancing from top to bottom) inside stagnant superheated liquid. The motion of the interface between the buffer and the test liquid (elliptical gray area near the bottom) is due to the approach of the boiling front. Butane, $\Delta T_{\mathrm{nom}} = 55$ K, $u_{\mathrm{fr}} = 0.76$ m/s, $d_{\mathrm{pipe}} = 80$ mm.

remained almost stationary for some time in a highly irregular manner. Figures such as this one show that although the entire liquid volume became superheated within a few milliseconds, it remained in this metastable state until the boiling front arrived. The front velocity of approximately 0.76 m/s was orders of magnitude lower than the sonic speed of depressurization in the pipe.

3.2. Close-up view of the boiling front

Fig. 3 gives an enlarged view of the boiling-front region. Again, the superheated liquid is at the bottom (white area) of the frame, while two-phase flow is accelerated towards the top. The boiling front where the explosive vaporization and fine-scale fragmentation occurred appeared to be several millimeters thick. Bubble-like structures covering a range of diameters up to a few millimeters grew and disappeared during front advancement into the metastable liquid. Smaller structures appeared on top of the larger bubbles and grew in turn. Bursts frequently occurred within the front and spread from one point to other locations. Because of this and the irregular shape of the boiling front, the resulting two-phase jet was not continuous and uniform near the front.

Fig. 4 shows a sequence of high-speed close-up views of the boiling front. Structures growing into the superheated liquid can be identified. The images, taken in the flattened pipe section mentioned above, do not allow identification of the expanding vapor cavities as either open caps or closed bubbles. However, they illustrate the repetitious cycle of bubble/cap generation and growth, growth of smaller structures on top of the larger ones, roughening of the surface and disappearance of the distinct structures. For example, the right side of frames 1–8 shows the growth of two larger structures. Reaching approximately three millimeters in diameter, smaller structures grow on their surfaces that become rough (frames 6–11). The boiling front then recedes locally (between frames 11 and 12) and several new smaller bubbles start growing again (frames 13

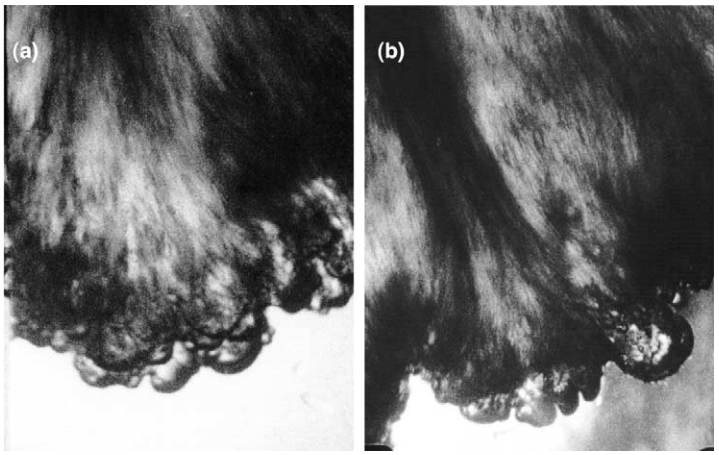

Fig. 3. Close-up views of boiling fronts advancing inside the stagnant superheated liquid, from top to bottom of the flattened test section. Propane, Runs 121 and 122, nominal superheats 50 and 49 K, left and right, respectively. The horizontal dimension of the photograph is approximately 21.5 mm.

and following) in a way reminiscent of fractal geometry. Similar successions of events can be seen in other parts of the field of view.

3.3. Transition from single-bubble growth to violent boiling with front propagation

The violent vaporization and/or fragmentation of liquid at the boiling front made the phenomena distinctively different from "slow" evaporation or smooth single-bubble growth

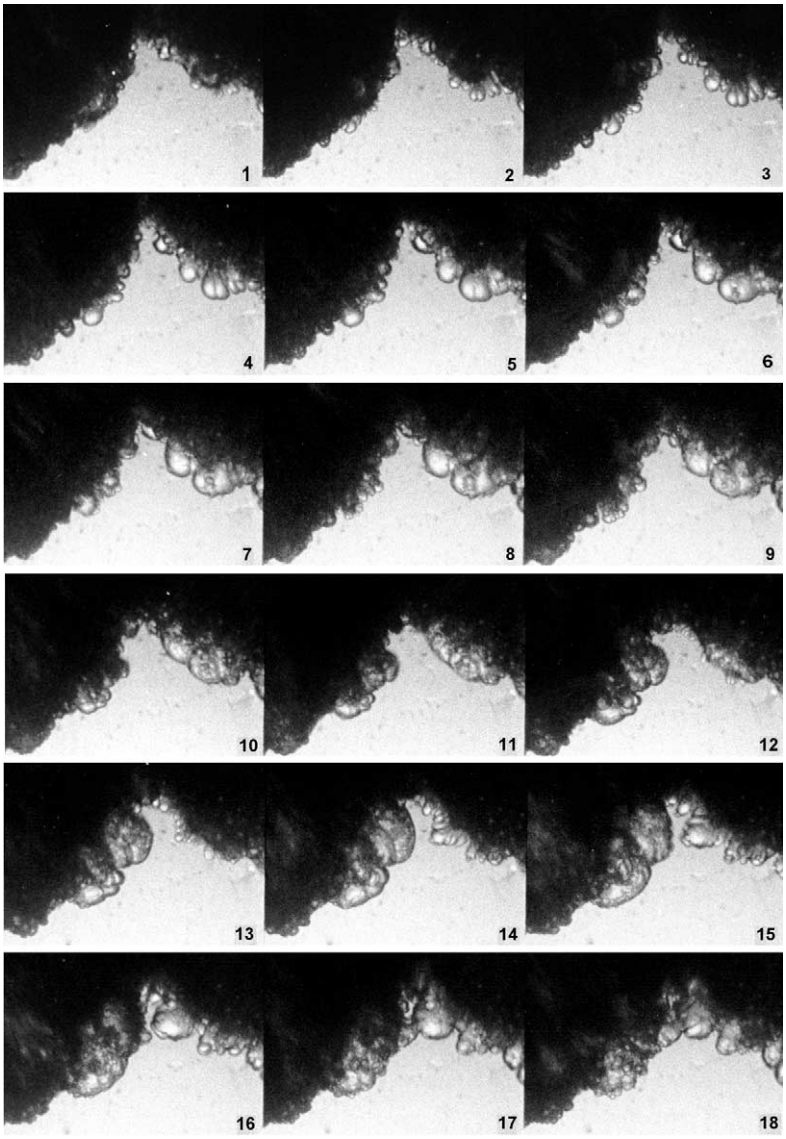

Fig. 4. Boiling front propagation in a flattened pipe (Run 121, propane, $\Delta T_{nom} = 50$ K, $u_{fr} = 1.2$ m/s, frame rate 4700 Hz, view field 35 mm × 24 mm).

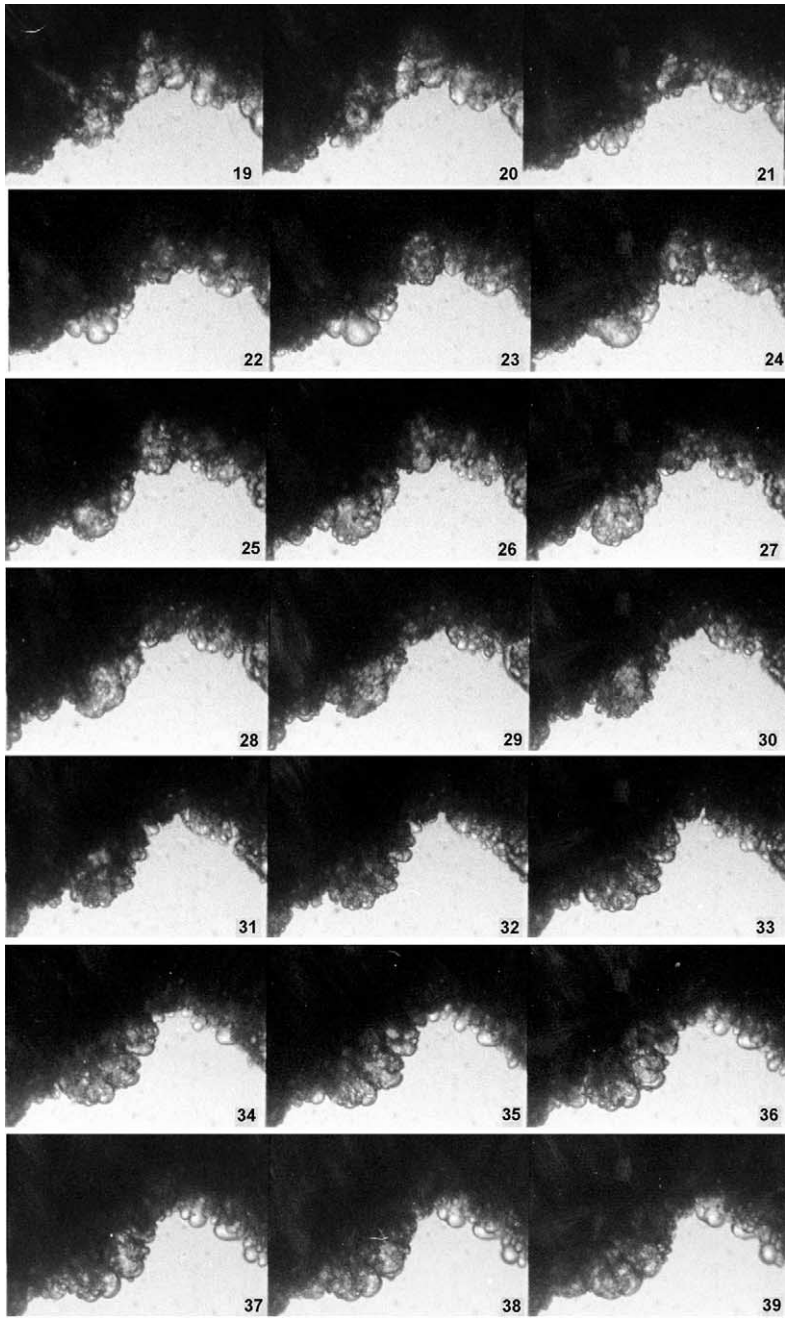

Fig. 4. *(Continued)*

phenomena. In one experiment, a transition from "normal" vaporization to violent boiling front propagation from the interface of a single-growing bubble was inadvertently produced; the study of this transition contributed to the understanding of boiling front propagation. This transition

was filmed in a flattened pipe and is shown in Fig. 5. The sequence of close-up frames shows part of the expanding bubble interface. The right side of the images is the vapor-filled interior of the bubble flattened between the two glass walls covered by a film of buffer liquid (water in this case). The left side shows the superheated liquid propane surrounding the bubble.

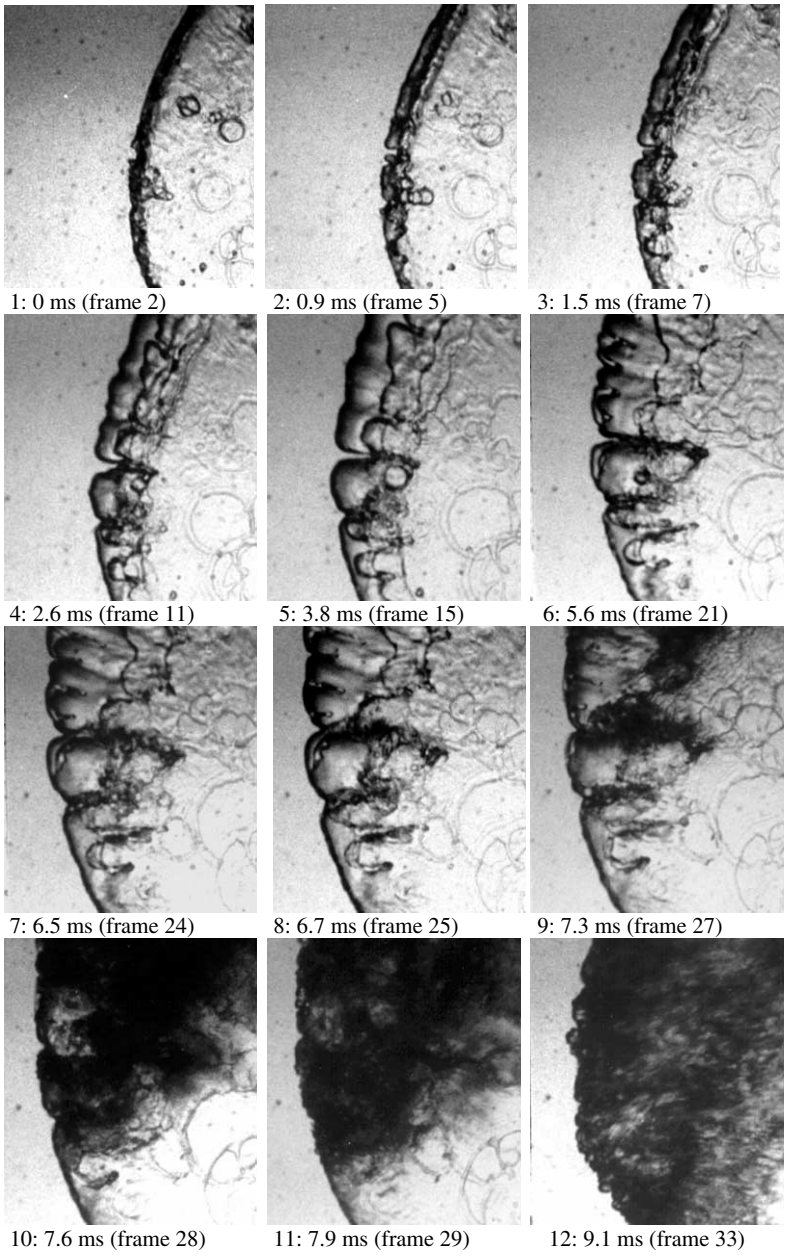

Fig. 5. Transition from pure vaporization to boiling front propagation at a bubble interface in a flattened pipe (propane, $\Delta T_{\text{nom}} = 63$ K, view field: 30 mm $\times$ 27 mm). Time steps shown are irregular.

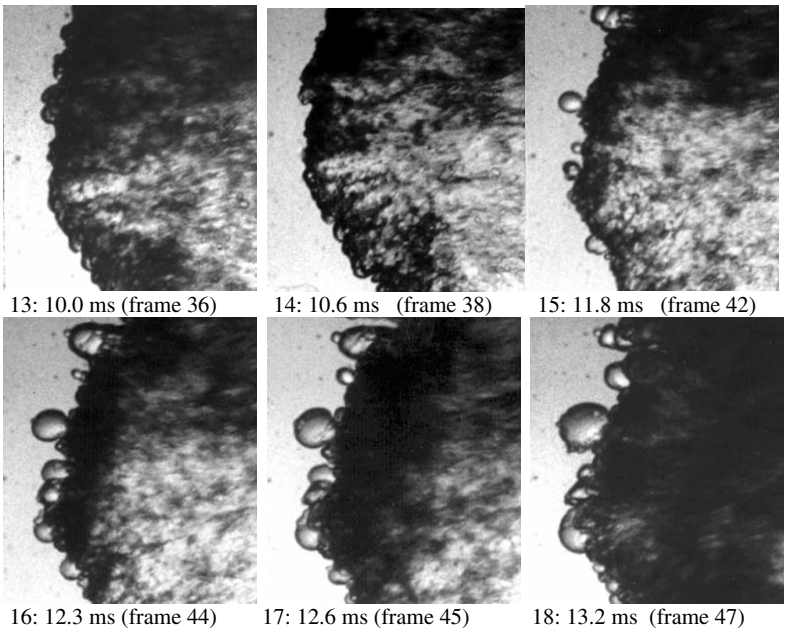

Fig. 5. *(Continued)*

In the first frame, the bubble has already grown to a diameter of approximately 30 mm. The ring patterns and structures visible within the bubble are probably due to vaporization of propane on the thin water film covering the wall. The bubble is still fully transparent at this stage, an indication that it consisted of pure vapor. As the interface moved from right to left, two folds or crevice-like structures accompanied by small ''bubbles'' appeared (near the center of the figure); these remained present in the following frames. Frames 2–7 show how the depth of these notches increased. In frame 9, small bubbly structures growing from the liquid notches became visible. On the next frame, explosive vaporization started. Including frames 11 and 12, it can be seen that, within a millisecond, the contour line of this structure disappeared and an expanding dark fog-like zone appeared. Frames 9–12 were taken in time steps of 0.29 ms. The observed change in transparency was probably due to fine-scale fragmentation. Small particles (below film resolution) and acceleration of this aerosol led to complete light refraction. A similar process occurred in the upper part of the frame, i.e., a zone of complete light extinction spread at the fold of two vapor cavities. A washboard-like ripple pattern can be seen along the stretched aerosol zone and away from the side of the superheated liquid (upper third of frame 10). This indicates a high relative motion of gas over the surface of the liquid film remaining on the glass walls. The next frames 10–14 show the rapid spread of the aerosol-generating sites. Away from the interface, the aerosol streamed towards the right and filled up the former bubble volume. Caps smaller than before could now be observed at the boiling front. A two-phase flow sped away from the front and the typical structure of a boiling front was finally established.

Some of the above phenomena, such as ripple formation, may have been an artifact caused by the narrow cross-sectional area of the glass receptacle and the shearing forces on the film between the glass wall and the vapor stream. Such a behavior may not be found in a ''wall-free'' envi-

ronment. However, the observation of explosive boiling and fine-scale fragmentation starting preferentially in the fold between neighboring bubble hemispheres was supported by a number of other close-up studies.

The prevailing explosive vaporization phenomena taking place during boiling front propagation can be summarized from recordings such as these of Figs. 3–5. It appears that liquid/vapor fronts at high superheat and moving rapidly generate a dramatic increase of their surface area. This in turn leads to increased vaporization, which in general induces a higher local motion between gas and liquid. Due to intense mixing and fragmentation, warmer liquid from the vicinity of the front is rapidly moved to the free surfaces. Thus, at high superheat, shortly after its initiation, explosive boiling appears as a self-amplifying process. The phase change proceeds as a self-sustaining mechanism, continuously generating new surface area for further vaporization. The phenomena examined in detail here are in agreement with previous observations such as those of Hill and Sturtevant (1990).

3.4. Influence of the superheat on the appearance of the boiling front

As shown later, increasing the superheat led to higher boiling front velocities, u_{fr}. The appearance of the front also changed. The size of the leading bubbles, starting from several millimeters, decreased with temperature. Therefore, the approaching front had a finer structured surface at high superheat. Fig. 6 compares the appearance of butane boiling fronts at $\Delta T_{nom} = 69$ K (frame (a)) and 32 K (frames (b)–(d)). The structures appearing in frame (b) (lower superheat) are coarser than those of the higher-superheat frame (a).

Frames (c) and (d) of Fig. 6 show the structures evolving in the stagnant superheated liquid at a temperature slightly below the onset of boiling front propagation. In this case, vaporization was much slower and some convection and mixing inside the superheated liquid could be observed. Indeed, at low superheat and consequently at low vaporization rate, (e.g., low-superheat run of Fig. 6), the vaporization that started at the free surface caused the liquid to cool down. An uneven distribution of local bubble growth and the resulting differences in density caused fluid motion,

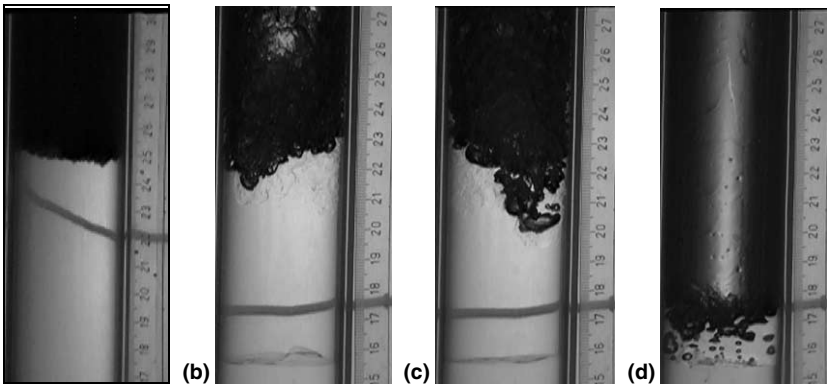

Fig. 6. Views of the boiling front at two different superheats; butane; view field: 125 × 60 mm. Frame (a): sustained boiling front propagation; $\Delta T_{nom} = 69$ K, $u_{fr} = 1$ m/s. Frames (b)–(d): slow boiling with liquid motion underneath the interface and residual, saturated (“cold”) liquid; at different time steps (0, 0.1 and 2.3 s); $\Delta T_{nom} = 32$ K, $u_{fr} = 0.045$ m/s.

which led to convective heat transfer from the bulk of the liquid to the free surface. The decrease in temperature is indicated by changes in the refractive index, visible near the boiling front in frames (b) and (c) of Fig. 6. Since, in this case, the latent heat and vapor production were not sufficient to carry away any surplus cooled liquid, and the process was much slower, mixing occurred, and the volume from which heat was removed increased. As the superheat near the interface was depleted, the heat required for vapor production had to be transported over an increasingly larger distance from the lower layers of the liquid to the liquid-vapor interface. Eventually, convective liquid motion affected the whole column of liquid through which the vaporization zone slowly propagated. At the end, a volume of saturated or "cold" liquid was left in the pipe (frame (d)). Reinke (1996) summarizes the qualitative findings and their dependence upon the superheat.

4. Quantitative results for boiling front propagation

The boiling front velocity and the pressure in the superheated liquid below the front were measured. The influences of geometry, superheat, and pressure on the phase change process were systematically investigated. The use of different fluids allowed the effect of fluid properties to be quantified.

4.1. Boiling front velocity

The contour of the boiling front changed continuously (Reinke, 1996), as shown in Fig. 2. Averaging over time and space the boiling-zone contour, the mean velocity of the front u_{fr} could be determined. Although locally and temporarily strong fluctuations were observed in the appearance of the flashing layer, the front traveled at a constant average velocity (Reinke, 1996) in agreement with observations of other investigators. The average velocity of the fronts, which was of the order of 1 m/s, was three orders of magnitude lower than the speed of sound in the pure liquid. This shows that the rate of depressurization and propagation of the phase-change front into the superheated liquid are totally decoupled processes.

4.2. Effect of flow cross-sectional area on boiling front velocity

To assess the applicability of the results to other geometries and scales, it is important to study the influence of the test-cell geometry on boiling front velocity. The impact of the diameter on front velocity was investigated by installing pipes of different sizes in the experimental setup of Fig. 1. The glass funnel provided additional investigations of the effect of diameter: with the front moving from top to bottom of the funnel, a single run allowed investigations in a continuously varying cross-section.

Within the range of circular internal pipe diameters 14–80 mm investigated, no significant influence of cross-sectional area on boiling front velocity became evident (Reinke, 1996). However, as the pipe diameter decreases down to the scale of the bubbly structures at the boiling front, the behavior of the front is significantly influenced by the presence of the glass walls; the front moves faster in a smaller diameter. This observation is consistent with the findings of, e.g.,

Sugioka (1991) who placed glass beads 0.4–0.7 mm in diameter in columns of refrigerants R-12 and R-114. The boiling front, traveling through the superheated liquid in this sphere bed, attained velocities six times greater than that without packing. The absence of nucleation sites on the walls of our test sections could also be reducing any dependence of the phenomena on test section diameter.

4.3. Effect of the cross-sectional area on the threshold of front propagation

The boiling front velocity was found to be independent of cross-sectional area in the present work, as noted above. According to Grolmes and Fauske (1974), however, the onset temperature for sustained front movement is influenced by the pipe diameter. In a systematic investigation of the diameter effect with methanol and refrigerant R-11, they found a decrease of the threshold superheat from approximately 53 to 23 K and from 59 to 28 K, respectively, with the pipe diameter increasing from 2 to 20 and 50 mm: their findings suggest an asymptotic threshold value at larger pipe diameters.

In the present work, the threshold was determined by extrapolating the correlated data trends to $u_{fr} = 0$ m/s. Since the pipe diameters used in this work were typically larger than those of Grolmes and Fauske (1974), it can be assumed that the thresholds in Fig. 7 are close to asymptotic values. As the effect of nominal versus real superheat vanishes when the front velocity tends to zero, there is no significant difference between the threshold values obtained by extrapolating with either nominal or real superheat.

4.4. Effect of nominal superheat on boiling front velocity

The test substances were always released to atmospheric pressure. The nominal superheat (as defined by Eq. (1)) was varied by changing the initial fluid temperature. The results are summarized in Fig. 7.

Characteristic similarities were observed for all four fluids. Above a certain threshold, the boiling front velocity increased linearly with superheat. The maximum observed speed of 1.3 m/s was reached with butane at $\Delta T_{nom} = 73$ K. Below the threshold there was no front propagation, but rather "quiet boiling" as shown in Fig. 6(b)–(d). Apparently, below the threshold, the stored and released latent heat is not sufficient to produce a vapor stream strong enough to carry away the surplus liquid.

The dependence of the front velocity on nominal superheat was correlated by linear regression. The resulting straight lines and the corresponding equations, together with the 20% error limits are plotted in Fig. 7.

For water, at superheats above about 20 K, the front velocity departed from the linear trend noted for the other test fluids and increased much more slowly with superheat. Initially, it was thought that, at high superheat, the two-phase water mixture downstream from the front was choked, producing higher front pressures and lower front velocities. Reinke (1996) showed, however, that the mass fluxes were too low to be critical. The front pressures computed with the method discussed later were also in agreement with the measured ones. No explanation could be found for the particular behavior of water. The linear regression of Fig. 7 considers only the low-superheat water data.

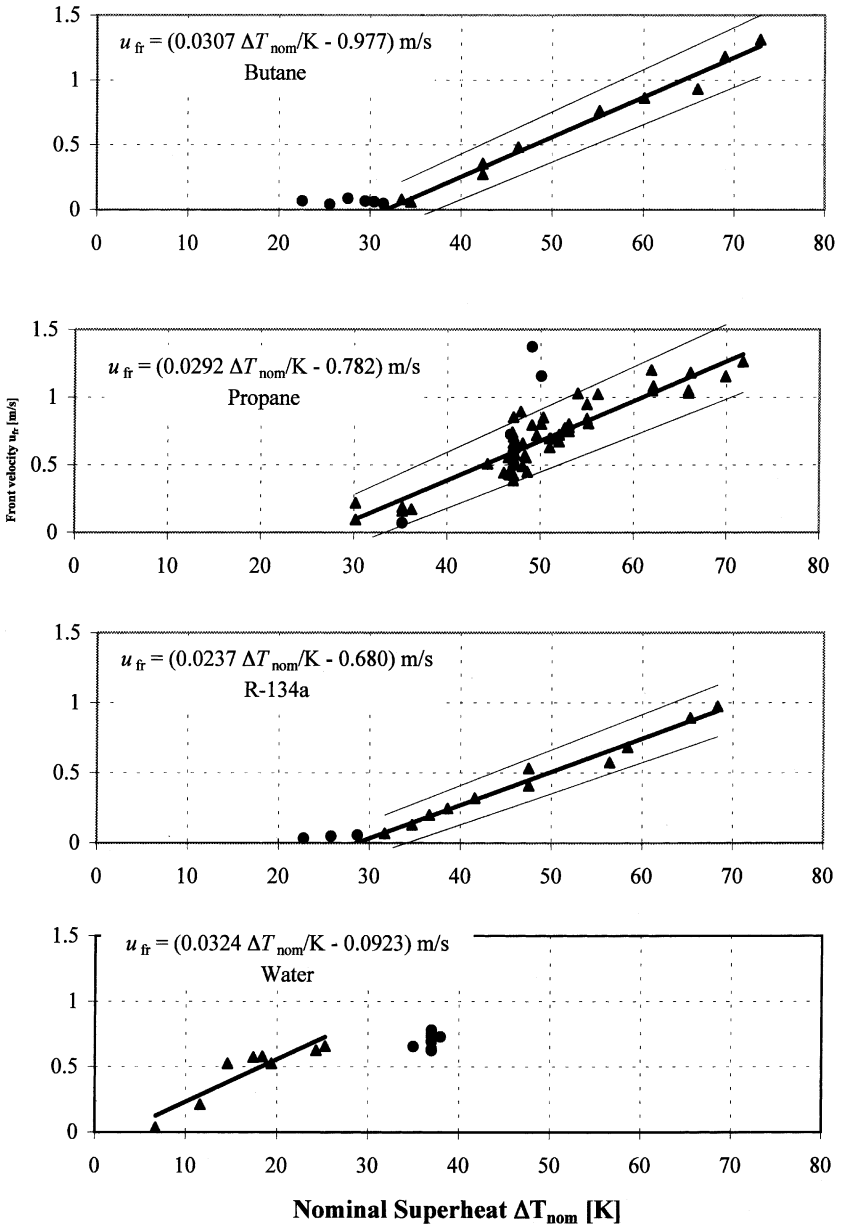

Fig. 7. Velocity of boiling fronts for butane, propane, R-134a and water (▲/●: data used/not used for linear correlation). Lines indicate linear regression and 80% confidence limits.

4.5. The pressure in the superheated liquid

As a consequence of quasi-steady boiling front propagation, the pressure upstream of the vaporization zone and other quantities showed rather stationary features as well. This can be seen in Fig. 8 that shows the recordings of the two pressure transducers. These were located in the

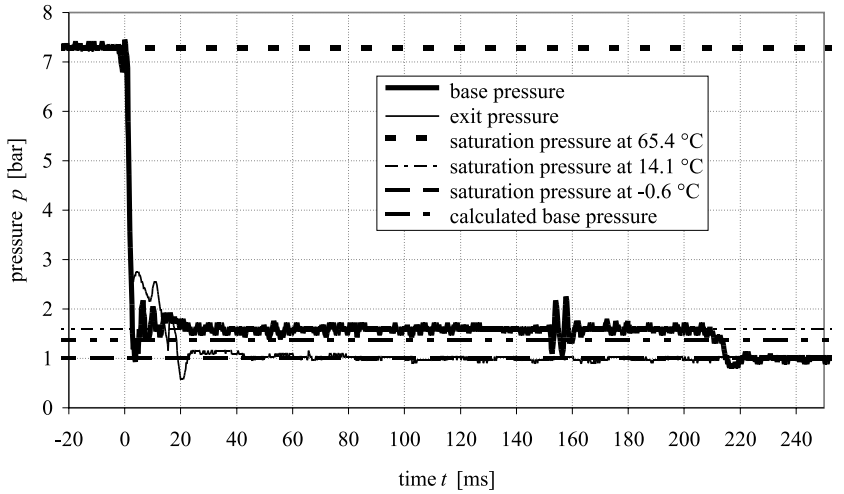

Fig. 8. Typical base and exit pressure traces during the release of superheated liquid with boiling front propagation (Run 092, butane, $\Delta T_{\text{nom}} = 66$ K, $u_{\text{fr}} = 0.93$ m/s. Calculated base pressure according to Eq. (14)).

buffer liquid below the test fluid and in the vapor space underneath the RD, respectively. After the sudden initial drop, a pressure plateau was recorded that corresponds to the period of quasi-steady boiling front propagation. After opening the glass pipe, the pressure at the exit decreased to the ambient pressure within 20 ms, whereas the pressure at the base remained at a plateau above the surrounding pressure for 200 ms. The pressure fluctuations are attributed to the combined effects of reflected pressure waves and randomly occurring bursts in the boiling zone.

The elevated pressure below the boiling front ("base" or "front" pressure) was due to the acceleration of the fluid and pressure losses between the surface of the superheated liquid and the exit of the pipe. This elevated pressure led to a smaller degree of real superheat, ΔT_{real}, (as defined by Eq. (2)) in the stagnant metastable liquid. In the example of Fig. 8 the nominal superheat $\Delta T_{\text{nom}} = 66$ K was thus reduced to $\Delta T_{\text{real}} = 51.3$ K.

In a few experiments an orifice was installed at the exit of the test pipe. The effects of the increased front pressure produced by the orifice will be discussed later.

5. Analysis of the boiling front experiments

5.1. Conservation equations for boiling fronts

To estimate the pressure in the liquid during depressurization, the front can be considered as a one-dimensional discontinuity of negligible thickness moving with the front velocity u_{fr}. Although violently unstable at the microscopic level, the front is assumed to progress at steady speed. The control volume of Fig. 9 is entered by superheated liquid (1) from the left with velocity $u_1 \approx u_{\text{fr}}$. Frictional effects are ignored and adiabatic flow is assumed. The two-phase flow leaving on the right (2) is assumed to be a homogeneous stream at u_2, which is approximated by the two-phase velocity u_{TPF} in an *absolute* frame of reference. In reality, $u_2 = u_{\text{TPF}} + u_{\text{fr}}$. However, since $u_{\text{TPF}} \gg u_{\text{fr}}, u_2 \approx u_{\text{TPF}}$ is a good approximation.

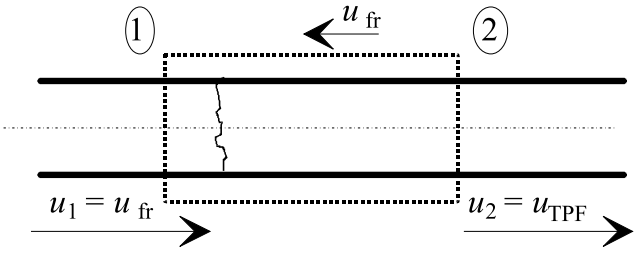

Fig. 9. Control volume used for analysis.

The upstream and downstream states are related by the following equations of conservation of mass, momentum and energy (in terms of enthalpy, h).

$$\rho_1 u_1 = \rho_2 u_2, \tag{3}$$

$$p_1 + \rho_1 u_1^2 = p_2 + \rho_2 u_2^2, \tag{4}$$

$$h_1 + \frac{1}{2}u_1^2 = h_2 + \frac{1}{2}u_2^2. \tag{5}$$

With equal velocities between the phases at 2, the two-phase density ρ_2 is given by

$$\frac{1}{\rho_2} = (1 - x_2)\frac{1}{\rho_{L2}} + x_2\frac{1}{\rho_{G2}}, \tag{6}$$

where x_2 is the flow quality at 2. The enthalpy at 2 is given by

$$h_2 = (1 - x_2)h_{L2} + x_2 h_{G2}, \tag{7}$$

where the indices L and G denote liquid and vapor, respectively. The properties at state 1, ρ_{L1} and h_1, are to be defined at T_1 while $h_{L2}, h_{G2}, \rho_{L2}, \rho_{G2}$ correspond to the saturated state at p_2.

For a given initial temperature T_1 and an exit (release or reservoir) pressure p_2 (for our experiments, the atmosphere, 1 bar), the above formulation of the *three* conservation equations, contains *four* unknowns, u_{fr}, u_{TPF}, p_1 and x_2. We used the measured u_{fr} and T_1 values to calculate the quality x_2.

Considering the fact that $\rho_{L2}/\rho_{L1} \approx 1$, Eqs. (3)–(7), lead to a quadratic expression for x_2

$$x_2^2 + \frac{\left(h_{LG2}/u_{fr}^2\right) - 1 + (\rho_{L1}/\rho_{G2})}{\frac{1}{2}(1 - (\rho_{L1}/\rho_{G2}))^2}x_2 - \frac{2(h_{L1} - h_{L2})/u_{fr}^2}{(1 - (\rho_{L1}/\rho_{G2}))^2} = 0 \tag{8}$$

with the vaporization enthalpy $h_{LG2} = h_{G2} - h_{L2}$.

Since typically $h_{LG}/u_{fr}^2 \gg \rho_L/\rho_G \gg 1$, Eq. (8) can be simplified to read

$$x_2^2 + \frac{2h_{LG2}}{u_{fr}^2(\rho_{L1}/\rho_{G2})^2}x_2 - \frac{2(h_{L1} - h_{L2})}{u_{fr}^2(\rho_{L1}/\rho_{G2})^2} = 0. \tag{9}$$

This equation yields the following approximate expression for the quality

$$x_2 = -L + L\sqrt{1 + \frac{2Ja}{L}}, \tag{10}$$

where Ja is the Jakob number defined as

$$Ja := \frac{h_{L1} - h_{L2}}{h_{G2} - h_{L2}} \tag{11}$$

and

$$L = \frac{h_{LG2}}{u_{fr}^2 (\rho_{L1}/\rho_{G2})^2}. \tag{12}$$

Study of Eqs. (9) or (10) indicates that for a given nominal superheat, i.e. initial temperature and corresponding enthalpy h_{L1}, a very broad range of boiling front velocities u_{fr} is obtained with only slight changes in the quality x_2 (Reinke, 1996). This corresponds also to large variations in the two-phase flow velocity.

Once the quality x_2 is known, the homogeneous two-phase flow velocity u_{TPF} can be obtained

$$u_{TPF} = \left(1 + x_2 \left(\frac{\rho_{L1}}{\rho_{G2}} - 1\right)\right) u_{fr}. \tag{13}$$

The momentum equation (4) provides the acceleration pressure drop Δp

$$\Delta p = p_1 - p_2 = \left(\frac{\rho_{L1}}{\rho_{G2}} - 1\right) \rho_{L1} x_2 u_{fr}^2. \tag{14}$$

Reinke (1996) examines the relationships between all the quantities considered above in detail. The predictions of Eqs. (13) and (14) will be compared with experimental results below, and the calculated values of the base or front pressure will also be used to further correlate the data in terms of the real superheat calculated from Eq. (2) with $p_L = p_1$. In general, the superheat is reduced significantly due to the increased pressure in the liquid behind the boiling front. Since the violent vaporization takes place within the boiling front region, the superheat that is actually controlling the phenomena must lie somewhere between the two values.

5.2. Description of the superheated liquids

For an adiabatic depressurization producing a metastable liquid state, the Jakob number Ja, defined by Eq. (11) above, gives the possible equilibrium-phase-change vapor mass fraction. It is defined as the ratio between the superheat energy available and the heat necessary for full vaporization of the saturated liquid after depressurization.

For initial (1) and final (2) states at rest, Ja is identical to the isenthalpic mass fraction or *isenthalpic flash fraction, x_h*. Assuming constant liquid heat capacity c_{pL} and using the vaporization enthalpy $h_{LG2} = h_{G2} - h_{L2}$

$$Ja = \frac{c_{pL} \Delta T_{12}}{h_{LG2}}. \tag{15}$$

Frequently, the Jakob number is multiplied by the liquid/vapor density ratio to yield the modified form

$$Ja^* = \frac{c_{pL} \Delta T_{12}}{h_{LG2}} \frac{\rho_{L2}}{\rho_{G2}}. \tag{16}$$

The Jakob number of most metastable liquids is below unity, that is, adiabatic flashing cannot vaporize all the liquid.

5.3. Difference between isenthalpic and isentropic flows

An *isentropic flash fraction* x_s can also be defined using the specific entropy s

$$x_s = \frac{s_{L1} - s_{L2}}{s_{G2} - s_{L2}} < Ja = x_h = \frac{h_{L1} - h_{L2}}{h_{G2} - h_{L2}}. \tag{17}$$

The definition of the isenthalpic quality assumes that the vapor/liquid mixture is at rest after vaporization; this results in the highest possible quality since no latent heat is converted to kinetic energy. In contrast, the isentropic quality results in maximum conversion to kinetic energy, thus leading to the lowest quality. The quality values for propane (calculated from Eq. (8) using the measured boiling front velocity regression line of Fig. 7 for u_{fr}) are between these two limiting cases, as shown in Fig. 10, and very near the isenthalpic line. Similar results are obtained for the other fluids. Therefore, *the phase-change at the boiling front cannot be described as an isentropic process*, as often proposed. Recalling the sensitivity of the two-phase flow velocity to quality changes noted above, it becomes obvious that the assumption of isentropic phase change will lead to considerable overestimation of the two-phase flow velocity.

5.4. Upstream pressure results

The experimental measurements of the boiling front velocity u_{fr} and the calculated values of x_2 from Eq. (8) were used to calculate the acceleration pressure drop Δp across the boiling front with Eq. (14). This pressure drop must be close to the difference measured between the pressure transducers in the stagnant liquid and at the exit (where we always measured $p_2 \approx 1$ bar). As an example, the calculated pressure p_1 was plotted in Fig. 8 and found to be somewhat lower than the

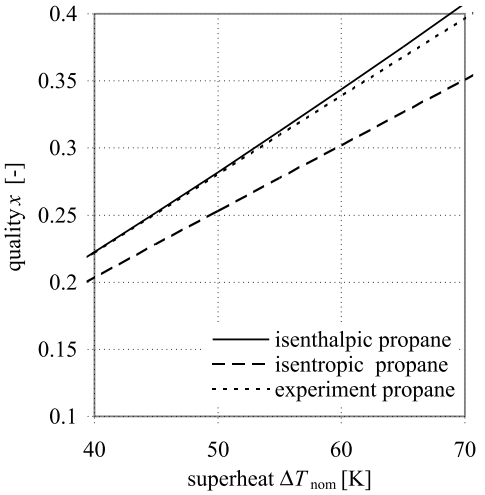

Fig. 10. Isenthalpic, isentropic and experimental quality x, for propane.

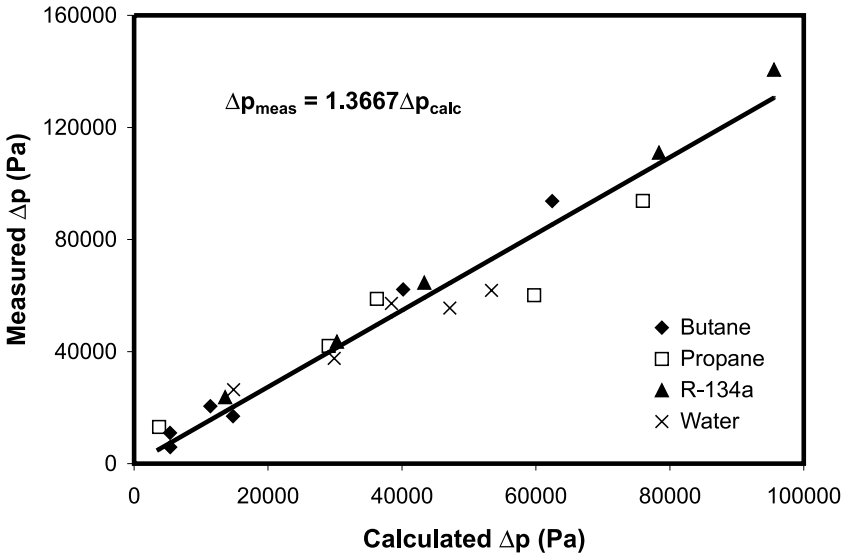

Fig. 11. Comparison of the pressure drops predicted with Eq. (14) with measured values.

measured value. Several runs were analyzed, using the measured boiling front velocity and the relevant fluid properties. The results are compared in Fig. 11.

The measurements of the base or front pressure p_1 during the period of constant boiling front propagation are found to be somewhat lower than the theoretical predictions. This is most likely due to the frictional, form, and gravitational pressure drops in the pipe, between the boiling front and the exit of the test section, that were not considered in the analysis. The general trend is well predicted, however, suggesting that the control-volume analysis is valid. Markedly different behavior by any of the fluids used cannot be observed. An analysis considering slip flow would have resulted in even lower theoretical pressure drop predictions (Reinke, 1996).

To obtain good predictions of the pressure at the boiling front for the subsequent analysis and correlation of the experimental data, an empirical correction was applied to the pressure drop across the boiling front calculated with Eq. (14). When the measured values were plotted against the calculated values, straight lines were obtained; this is not surprising since any frictional or form pressure drop would be proportional to the values predicted by Eq. (14). Although somewhat more accurate correction factors could be obtained for each fluid separately (ranging between 1.23 and 1.51), the best-fit line through all the available data yielded a correction factor of 1.367. (This suggests a loss coefficient of 0.733.) In the following work, the pressure at the front was calculated considering this correction factor.

5.5. Two-phase flow velocity

In a number of experiments, the velocities of the boiling front and of the mist stream flowing approximately 0.9 m downstream of the front were measured simultaneously (Reinke, 1996). The mixture velocity was estimated as the measured velocity of the droplets. Two-phase flow velocities u_{TPF} calculated using the control-volume analysis presented above were compared to the exper-

imental estimates. The *measured* liquid droplet velocities were lower than the calculated ones. The difference was significant, in particular at low velocities. This could be attributed to the assumption of homogeneous flow: at low superheat and correspondingly lower mixture velocity, differences between the mixture (or vapor) velocity and the velocity of the liquid drops may be significant, but difficult to quantify analytically in a situation such as the one considered here.

6. Quantitative prediction of boiling front behavior

Vapor generation could not be clearly attributed to any single instability or nucleation mechanism, but is most likely the combined effect of several interacting phenomena (Reinke, 1996). Both secondary nucleation and the hydrodynamic instability mechanisms of Rayleigh–Taylor, Kelvin–Helmholtz and Landau (Prosperetti and Plesset, 1984) could possibly be, at least partly, responsible for the process of surface generation, vaporization and liquid fragmentation.

Two different vaporization mechanisms appeared clearly in the experiments: slow bubbling below a certain threshold and boiling front propagation above a certain superheat. Thus, the analysis was separated into two steps: determination of the onset or threshold temperature for front propagation, and prediction of the front velocity as a function of the superheat. Because of the complexity of the phenomena, the behavior of the front could only be correlated to the relevant parameters by non-dimensional analysis.

To conduct the non-dimensional analysis, all the likely relevant variables and fluid properties were considered and all possible non-dimensional numbers were systematically produced (Schmidli and Yadigaroglu, 1995). Numerous attempts were then made to detect systematic relationships between the non-dimensional numbers containing the threshold superheat and the front velocity and those containing the experimental conditions (initial temperature) and fluid properties. Numerous linear relationships, exponential and power laws were tried. The resulting successful and physically meaningful correlations are reported below.

6.1. Non-dimensional numbers

The original or the modified Jakob numbers, Ja or Ja^*, Eqs. (15) and (16), seem to be the natural non-dimensional numbers for scaling the superheat. The non-dimensional numbers that may be formed with u_{fr} are the capillary number Ca, a non-dimensional kinetic energy Nb, and two new numbers called Na and Nc proposed by Schmidli and Yadigaroglu (1995)

$$Ca = \frac{\mu_{\mathrm{L}} u_{\mathrm{fr}}}{\sigma}, \quad Na = \frac{\sigma u_{\mathrm{fr}}}{\lambda_{\mathrm{L}} \Delta T_{\mathrm{thr}}}, \quad Nb = \frac{u_{\mathrm{fr}}^2}{h_{\mathrm{LG}}}, \text{ and } Nc = \frac{u_{\mathrm{fr}} \lambda_{\mathrm{L}}}{\sigma c_{\mathrm{L}}}$$

Not considering the surface tension, the liquid Prandtl number Pr_{L} is the unique non-dimensional number combining fluid properties controlling both conduction of heat and viscous effects in the fluid. Inclusion in the analysis of the surface tension via a fluid-properties group such as the Ohnesorge number, Oh, requires the simultaneous introduction of a length scale. There is no obvious length scale for the present problem, except a front boundary layer thickness (Hill and Sturtevant, 1990)

$$\delta = \frac{\kappa_{\mathrm{L}}}{u_{\mathrm{fr}}},$$

where κ_L is the thermal diffusivity ($\kappa = \lambda/\rho c$) of the liquid. Using this scale in *Oh*, produces, however, only a combination of previously defined numbers

$$Oh = Pr_L^{0.5} Ca^{0.5}.$$

Thus, use of *Ca*, *Na*, *Nc* or *Oh* involves also the surface tension that is influencing the break-up properties of the fluid.

6.2. Choice of representative temperatures for the fluid properties

Fluid properties, in particular the properties of the gaseous phase, may change very significantly in the range between the initial fluid temperature and the saturation temperature at reservoir pressure; it is important to examine at which temperature the fluid properties should be evaluated. There are good arguments for choosing either the initial liquid temperature, T_{in}, or the saturation temperature corresponding to the reservoir or front pressure during vaporization. Although the bulk of the superheated fluid clearly remains at the initial fluid temperature, the temperature at the boiling front is likely to quickly reach the saturation temperature corresponding to the pressure at the front, $T_{sat,fr}$. Further downstream, the reservoir pressure and the corresponding saturation temperature are reached. The saturation temperature at reservoir pressure is very convenient for evaluating the fluid properties (since it requires no knowledge of the front pressure), but cannot be used for choked releases and for releases into very low-pressure reservoirs (as in certain experiments by others).

In agreement with the analysis of Section 5, at the threshold of boiling front propagation, the boiling front pressure tends towards the reservoir pressure; thus, at threshold conditions, the saturation temperature at reservoir pressure is also the front temperature. The superheat at the threshold of boiling front propagation could be correlated with the fluid properties taken T_{in} or $T_{sat,fr}$. The work discussed below showed, however, that best consistency and overall results could be obtained when the liquid properties were evaluated at T_{in} and the gas properties at $T_{sat,fr}$. The latent heat entering in the *Ja* numbers, Eqs. (15) and (16), was also replaced by $h_G(T_{sat,fr}) - h_L(T_{in})$. This "latent heat" represents the (lesser) enthalpy needed for vaporization of the superheated fluid. This choice is used throughout the following section, unless noted otherwise. It is logical, since it assigns T_{in} to the liquid below the boiling front and $T_{sat,fr}$ to the gas above the boiling front (corresponding to the saturation pressure there).

6.3. Correlations for the superheat at the onset of boiling front propagation

Correlations of the original and of the modified threshold Jakob numbers (*Ja* and Ja^*) versus Pr_L were successful. Our own data could be correlated with either one, but the *Ja* correlations produced inconsistent trends against the data collected by others. Although several alternative (Ja^*,Pr_L) correlations are possible, depending on the choice of temperature at which the fluid properties are evaluated, the following two led to the best results.

With *all* the fluid properties calculated at the *saturation temperature corresponding to the ambient reservoir* (*or, at the limit, front*) *pressure*, $T_{sat,fr}$, the modified Jakob number correlated the new data presented here very well (Fig. 12)

$$Ja^*_{thr} = 10.11 Pr_L^{0.971}. \tag{18}$$

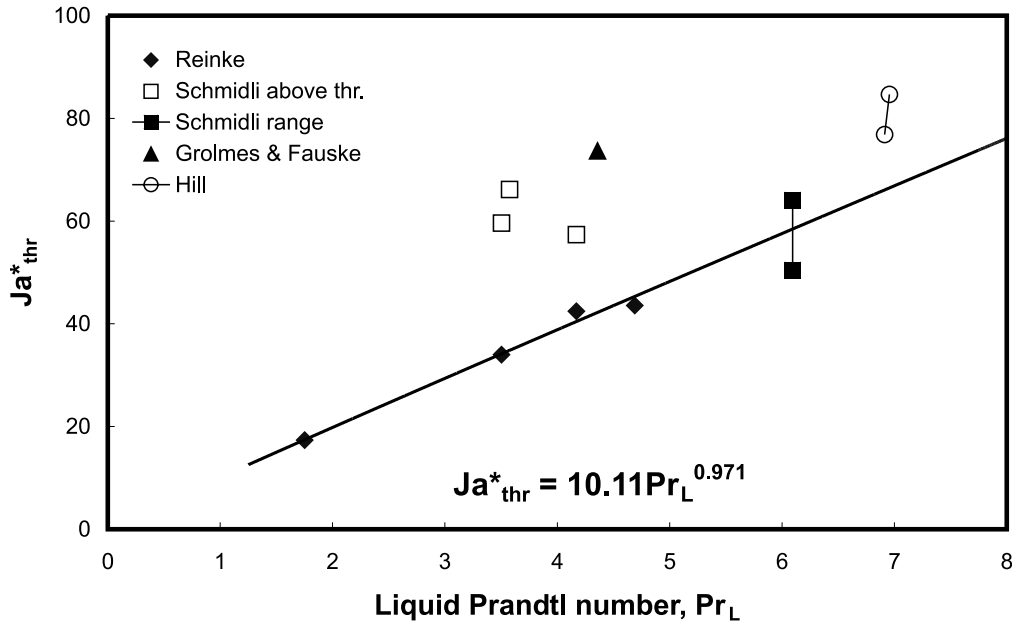

Fig. 12. Correlation of the measured threshold superheats (in terms of a modified Jakob number) with the Prandtl number of the liquid. All the fluid properties are evaluated at the saturation temperature corresponding to the front pressure. Data of other investigators are also included.

Alternatively, the data were also well correlated when the *liquid properties were obtained at the initial fluid temperature*, T_{in}, and the gas properties at $T_{sat,fr,}$ as noted in Section 6.2 (Fig. 13)

$$Ja^*_{thr} = 8.997 Pr_L^{1.325}. \tag{19}$$

The presence in the correlations and the relevance of the Prandtl number are not surprising, as already noted in Section 6.1. The surface tension is absent, but the experimental findings do not show any need for considering it. The Prandtl number is the ratio between the diffusivities for momentum and heat. The correlations indicate that the higher this ratio, the larger the superheat that can be sustained in the liquid before the creation of a boiling front.

Data obtained by other investigators are assembled in Table 1 and included in Figs. 12 and 13. For releases at sub-atmospheric pressure, the saturation temperature corresponding to the measured front pressure was used to calculate the fluid properties, when needed. As already noted, for our own experiments, since the threshold values are extrapolations to zero front velocity, there is no significant difference at the threshold between reservoir pressure and front pressure.

Hill (1991) performed releases of refrigerants R-114 and R-12 with initially saturated fluid at 20°C to a sub-atmospheric pressure reservoir. One of his R-114 points approaches the threshold condition of interest here. Hill reports both the test-section exit pressure (0.51 bar) and a somewhat higher pressure at the base of the liquid (0.54 bar). Hill's threshold superheat was 34.2 K (at base pressure) and 31.9 K at the exit pressure; a certain front velocity *was* measured under these conditions, however. Both points are plotted in the figures and lie near and above the

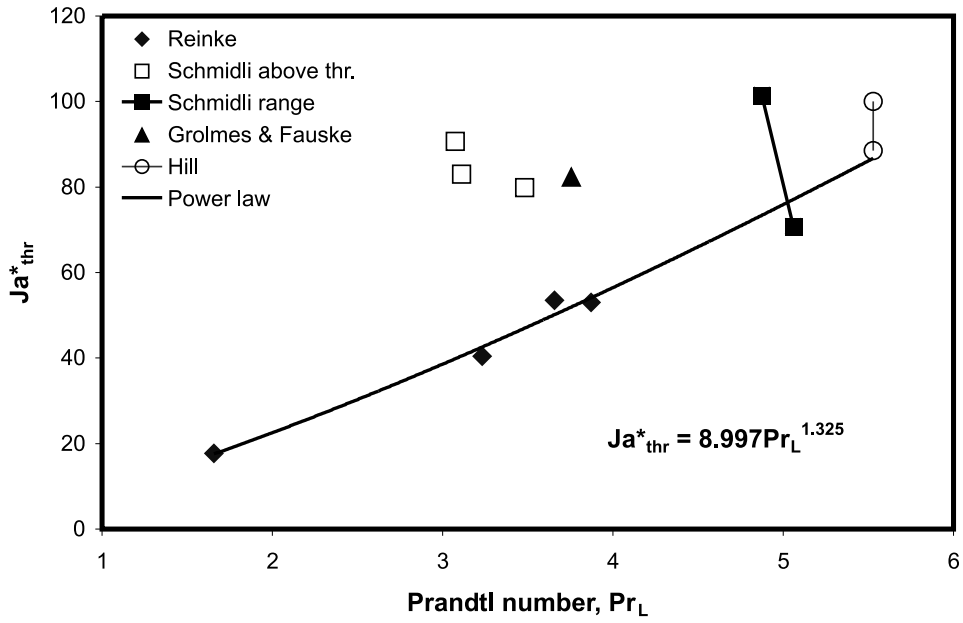

Fig. 13. Correlation of the measured threshold superheats (in terms of a modified Jakob number) with the Prandtl number of the liquid. The liquid properties are evaluated at the initial fluid temperature, while the gas properties at the saturation temperature corresponding to the front pressure. Data of other investigators are also included.

Table 1
Threshold superheat data used to create and test the correlations

Authors	Fluid	Reservoir pressure (bar)	Saturation temperature at reservoir pressure (K)	Threshold superheat (K)	Remarks
Reinke (this work)	Water	1.00	373.2	5.8	
	Propane		231.1	26.8	
	n-Butane		272.5	31.8	
	R-134a		247.1	28.7	
Schmidli (1993)	Propane	1.00	231.1	47	Above threshold
	R-12		243.1	52	
	R-114		276.5	37	Range: low and high limit
			276.5	47	
	n-Butane		272.5	43	Above threshold
Grolmes and Fauske (1974)	Methanol	0.075	283.2	20	Estimated values for largest diameters
	R-11	0.43	275.2	28	
Hill (1991)	R-114	0.51	259.8	34.2	With test section exit pressure
		0.54	260.5	31.9	With front pressure
	R-12	1.00	243.1	47.4	Above threshold

correlation line, as expected. For R-12, Hill's threshold was below 45 K but was not reached (this point is near another data point by Schmidli discussed next).

Schmidli (1993) released superheated liquid from shattered glass spheres to the atmosphere. The nominal threshold superheat was somewhere in the range 37–47 K for R-114; his points at the limits of this range are also shown in the figure and bracket the correlation line. Explosive vaporization was observed *above* nominal superheats of 47 K for propane, 43 K for butane, and 52 K for R-12. These values, also plotted in the figure (open symbols), lie above the correlation line, as expected again.

Two threshold data points obtained with methanol and R-11 by Grolmes and Fauske (1974) are also used. These are the values measured with the largest diameter used (but they could well still be above the asymptotic values for very large diameter). The R-11 point lies not too far above the correlation line, as expected again. The methanol point was obtained at very low reservoir pressure that drives the modified Jakob number very high; it is not plotted in the two figures (small differences in very low reservoir pressure create very large differences in the Ja^*).

The main conclusion that can be drawn from the above is that the correlations developed from our own data predicted also well the threshold superheats for several diverse experiments (including releases to sub-atmospheric pressure) by others. The results are quite sensitive to the values of the fluid properties and care should be taken in properly evaluating these.

6.4. Correlation for front velocity

Having obtained the threshold for boiling front propagation, the next step is to correlate the predominantly linear dependence of the boiling front velocity with superheat. The straight trend lines of Fig. 7 can be described by the threshold superheat ΔT_{thr} (or the threshold Ja_{thr} or Ja^*_{thr}) and the slope of the lines.

Although the nominal superheat is readily available, it is not the appropriate measure for choked releases and at very low reservoir pressure. Use of the real superheat, calculated with the (computed or measured) pressure at the front, is a better choice. The front pressure and the real superheats, Eq. (2), were computed for all data points using the procedure developed in Section 5, including the correction for friction.

Again, the choice of the proper temperatures for evaluating the fluid properties becomes important. *Our* front velocity data could be correlated using the properties at either T_{in} or $T_{\mathrm{sat,fr}}$ (for most of our data, the saturation condition at atmospheric reservoir pressure). But such correlations would not have been usable for the sub-atmospheric releases of others and for our own data obtained at higher pressures with the help of orifices. Regarding the choice of the proper temperatures for calculating the fluid properties, Hill's experiments provided useful hints: they were conducted at constant initial fluid temperature and variable reservoir pressure. They clearly show dependence on reservoir (or front) pressure. Thus, it does not seem reasonable to use *only* the initial fluid temperature for calculating all fluid properties. For the correlations proposed here, the "mixed approach" (liquid at T_{in}, gas at $T_{\mathrm{sat,fr}}$) outlined in Section 6.2 was used.

Since the relationship between u_{fr} and ΔT_{real} is predominantly linear, use of Nb is not justified. Our data sets for various fluids, plotted separately for each, produced straight lines in the (Ca, Ja) – but not in the (Ca, Ja^*) – plane. (Note that they could have also been correlated in the (Nc, Ja) plane; this is not surprising since $Ca = Nc\,Pr_{\mathrm{L}}$.) The approach that was successfully followed was

to correlate the threshold Ja_{thr} (and possibly also the slopes) of these lines with the Prandtl number of the fluid.

The best-fit straight lines to the data plotted in (Ja, Ca) planes provided threshold, Ja_{thr}, and slope values for each fluid. Care had to be exercised in including only points where boiling front propagation behavior was clearly evident. The water data could be fitted with a straight line only at low superheat, as visible in Fig. 7. (Plots of the data in (Ja^*, Ca) planes showed a non-monotonic (inverted "C" like) variation of Ca with Ja^*, making correlation impossible.) The Ja_{thr} values can be converted to Ja^*_{thr} values by multiplying them with $\rho_{\mathrm{L}}(T_{\mathrm{in}})/\rho_{\mathrm{G}}(T_{\mathrm{sat,fr}})$. As expected, the Ja^*_{thr} values obtained this way were in agreement with the ones delivered by Eqs. (18) or (19); the Pr_{L} was evaluated with liquid properties at threshold temperature.

The slopes of the correlation lines differed from fluid to fluid. The variation of the slope with Pr_{L} is not perfectly monotonic; thus the slope cannot be correlated in a fully satisfactory way with Pr_{L}. Thus, it seemed preferable to use an average slope in deriving a general correlation. A correlation of our data was obtained as

$$Ca = 0.0813(Ja - Ja_{\mathrm{thr}}), \quad Ja_{\mathrm{thr}} = Ja^*_{\mathrm{thr}} \frac{\rho_G(T_{\mathrm{sat,fr}})}{\rho_L(T_{\mathrm{in}})} \tag{20}$$

with Ja^*_{thr} calculated with Eq. (19). In Fig. 14 the measured Ca values are compared to the ones obtained from Eq. (20). Given the range of fluids tested, the uncertainties in the data, the difficulties in properly defining the fluid properties and the scatter of the experimental data, the agreement can be considered fairly satisfactory.

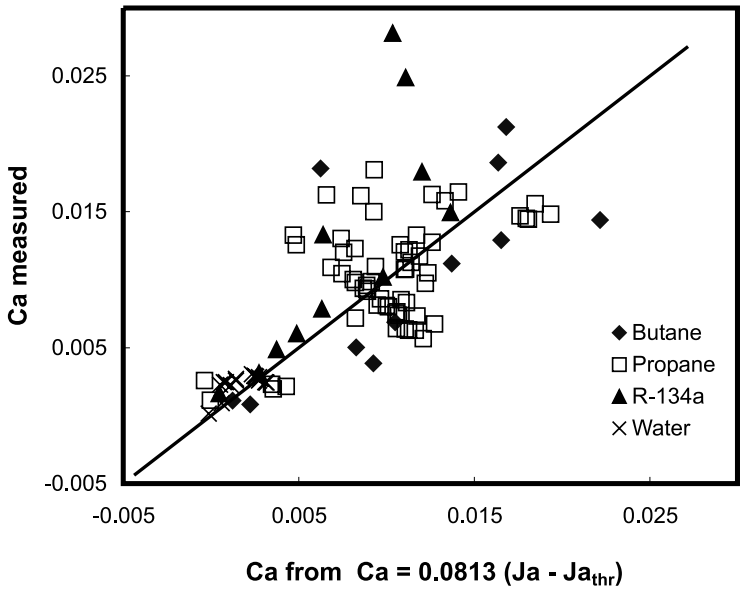

Fig. 14. Front velocities (presented in non-dimensional form as capillary numbers) predicted using Eq. (20) compared to measured Ca values.

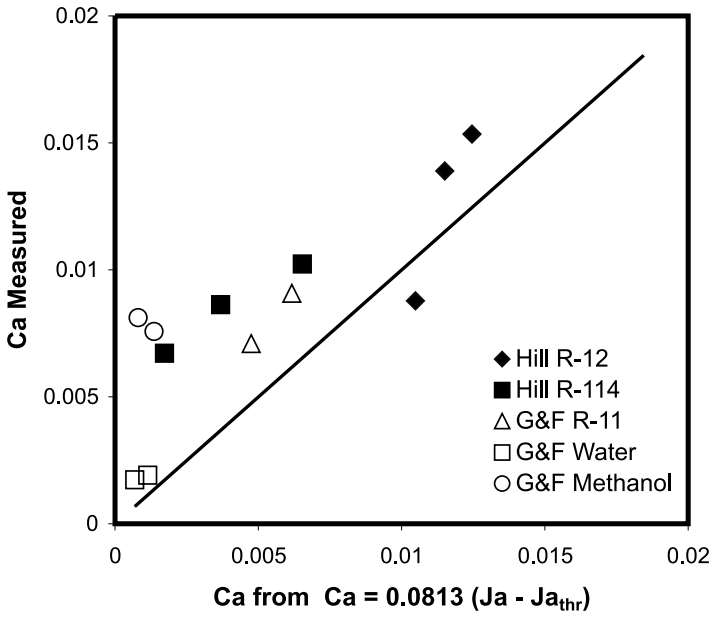

Fig. 15. Comparison of front velocities (in terms of *Ca*) predicted using Eq. (20) with values measured by other investigators.

A somewhat lesser scatter of the predicted data was obtained by correlating the threshold *Ja* numbers obtained from the (Ja, Ca) plots with the Prandtl number of the liquid

$$Ca = 0.0543(Ja - 2.930 \times 10^{-4} Pr_{\mathrm{L}}^{5.280}). \tag{21}$$

This correlation reveals, however, extreme sensitivity to the value of Pr_{L} that makes it unusable outside the original fluid range.

Fig. 15 compares the predictions made with Eq. (20) to the data of other investigators; these include the data of Hill (1991) obtained with R-12 and R-114 (three points each) and the older data of Grolmes and Fauske (1974) with R-11, water and methanol (two points each). These data involved releases to reservoirs at sub-atmospheric pressure. The agreement is not perfect, but given the great uncertainties in the data and the differences in the experimental procedures, again, fairly satisfactory.

Use of the correlations proposed here requires an iterative process: the boiling front velocity and the pressure at the boiling front must be obtained simultaneously using the correlations and the control-volume analysis of Section 5.1. The rates of vaporization obtained in this manner should be considered as minimum values. Indeed, in actual situations, nucleation may take place at multiple fronts (Reinke, 1996).

6.5. Effects of orificing

A small number of our experiments were conducted with an orifice installed at the exit of the test section, as mentioned in Section 2. Experiments with propane and butane conducted with and without an orifice are compared in Fig. 16. All the tests conducted without an orifice, in which the

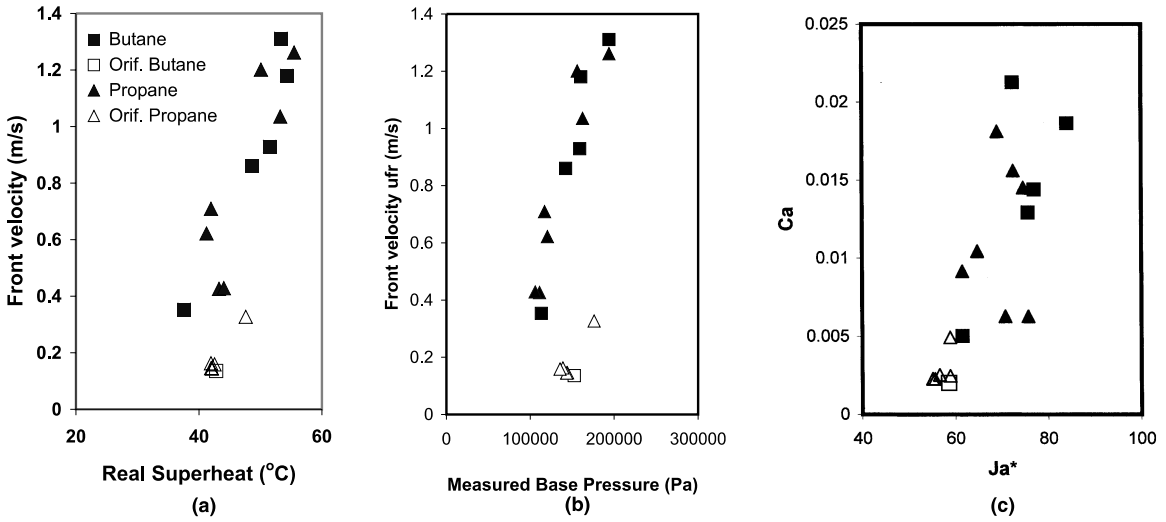

Fig. 16. Effect of orificing. (a) front velocities plotted versus the real superheat at the front. Front velocity (in terms of *Ca*) plotted versus: the pressure at the front (b), and the real superheat (in terms of Ja^*) (c).

base pressure was also measured, are reported in this figure. The orificing of the flow area from $d = 80$ mm to $d = 30$ mm resulted in higher pressure ($p_{fr} = p_l$) in the superheated liquid. The left plot presents the measured front velocities versus the real superheat computed with the measured base pressure. At the same real superheat, the higher base pressure led to reduced boiling front velocity in the experiments conducted with an orifice. The middle plot shows the front velocities plotted versus the measured front pressures. The data with and without orificing fall on the same curve, suggesting that the front velocity is not only controlled by the initial superheat, but by the front pressure as well. The front pressure depends, however, on the superheat. Finally the (Ca, Ja^*) plot on the right of Fig. 16 shows that when the data are considered in these non-dimensional coordinates, they again tend to fit together. The data obtained with the orifice produced much lower front velocities and lie much lower, but extend naturally beyond the cloud of points obtained without an orifice. In summary, Fig. 16 supports the validity of the correlation method presented here.

7. Conclusions

Boiling front propagation experiments were conducted systematically with four different fluids in nucleation-site-free glass receptacles. The thermophysical properties of the fluids covered a wide range. Extensive and detailed visual observations of boiling front propagation were made. The propagation apparently results from the interacting processes of vaporization, liquid fragmentation and fluid acceleration. The explosive nature of the boiling observed at the front was mainly attributed to the self-amplifying process of surface-area creation. The visual observations reveal a fractal-like process of bubble generation, smaller bubbles or vapor caps appearing inside larger ones.

The measured boiling front velocities varied predominantly *linearly* with the liquid superheat. Contrary to certain previous findings, a systematic study revealed no effect of pipe diameter on front velocity; this could possibly be attributed to the relatively large pipe diameters used in our experiments and to the complete absence of wall nucleation sites.

The velocity of the two-phase mixture created from the boiling front is lower than the value predicted assuming an isentropic expansion. Therefore, phase-change at the boiling front cannot be described as an isentropic process, as often proposed.

The pressure increase created at the boiling front by the momentum of the vaporizing fluid reduces the nominal superheat (i.e., the superheat with respect to reservoir pressure). This effect must be considered in the analysis of the data. A simple method based on the conservation equations applied to the boiling front, considered as a discontinuity, can be used to predict the pressure at the boiling front and the real superheat.

An analysis based on non-dimensional numbers led to successful correlations of our data: both the threshold for the appearance of a boiling front and the front velocity could be predicted using Jakob numbers for the superheat and Capillary numbers for the front velocity; the latter includes the surface tension of the liquid. Using the correlations derived from our own data, data of other investigators, as well as data obtained with an orifice at the exit of our test section, could be predicted fairly successfully. The correlation work revealed the importance of the proper choice of temperatures for evaluating the fluid properties.

Acknowledgements

This work was partly supported by the Swiss National Science Foundation under Contract No. 20-36145.92. The experiments were performed at the Paul Scherrer Institute in Switzerland; this support is gratefully acknowledged.

References

Barbone, R., Frost, D.L., Makris, A., Nerenberg, J., 1995. Explosive boiling of a depressurized volatile liquid. In: Waves in Liquid/Gas and Liquid/Vapour Two-Phase Systems, IUTAM Symposium, Kyoto, Japan, 1994. Kluwer Academic Publishers, Dordrecht, The Netherlands, pp. 315–324.

Blander, M., Katz, J.L., 1975. Bubble nucleation in liquids. AIChE J. 21, 833–848.

Das, P.K., Bhat, G.S., Arakeri, V.H., 1987. Investigation on the propagation of free surface boiling in a vertical superheated liquid column. Int. J. Heat and Mass Transfer 30, 631–638.

Frost, D., 1988. Dynamics of explosive boiling of a droplet. Phys. Fluids 31, 2554–2561.

Frost, D., Sturtevant, B., 1986. Effects of ambient pressure on the instability of a liquid boiling explosively at the superheat limit. J. Heat Transfer 108, 418–424.

Grolmes, M.A., Fauske, H.K., 1974. Axial propagation of free surface boiling into superheated liquids in vertical tubes. In: Proceedings of the Fifth International Heat Transfer Conference (Japan Soc. Mech. Eng., Soc. Chem. Eng.), Paper B1.7, Vol. 4, Tokyo, Japan, pp. 30–34.

Hill, L.G., 1991. An experimental study of evaporation waves in a superheated liquid. Doctoral Thesis, California Institute of Technology, Pasadena, CA, USA.

Hill, L.G., Sturtevant, B., 1990. An experimental study of evaporation waves in a superheated liquid. In: Meier, G.E.A., Thompson, P.A. (Eds.), Adiabatic Waves in Liquid–Vapor Systems, IUTAM Symposium, Göttingen, Germany, 1989. Springer, Berlin, Germany, pp. 25–37.

Jarvis, T.J., Donohue, M.D., Katz, J.L., 1975. Bubble nucleation mechanisms of liquid droplets superheated in other liquids. J. Colloid Interface Sci. 50, 359–368.

McCann, H., Clarke, L.J., Masters, A.P., 1989. An experimental study of vapour growth at the superheat limit temperature. Int. J. Heat and Mass Transfer 32, 1077–1093.

Moore, G.R., 1956. Vaporization of superheated drops in liquids. Doctoral Thesis, University of Wisconsin, MD, USA.

Nguyen, V.T., Furzeland, R.M., Ijpelaar, M.J.M., 1988. Rapid evaporation at the superheat limit. Int. J. Heat and Mass Transfer 31, 1687–1700.

Peterson, R.J., Grewal, S.S., El-Wakil, M.M., 1984. Investigation of liquid flashing and evaporation due to sudden depressurization. Int. J. Heat and Mass Transfer 27, 301–309.

Prosperetti, A., Plesset, M.S., 1984. The stability of an evaporating liquid surface. Phys. Fluids 27, 1590–1602.

Reinke, P., 1995. Druckentlastungsvorrichtung mit Berstscheibe. Erfindungspatent für die Schweiz und Liechtenstein Nr. 685307, Bundesamt für geistiges Eigentum, Bern, Switzerland.

Reinke, P., 1996. Surface boiling of superheated liquid. Doctoral Thesis, No. 11598, Swiss Federal Institute of Technology, Zurich, Switzerland.

Reinke, P., 1997a. Site deactivation techniques for suppression of nucleation in superheated liquid. Exp. Heat Transfer 10, 133–140.

Reinke, P., 1997b. Mechanism for controlled, pressure-tolerant opening of a rupture disc. Kerntechnik 62, 262–263.

Schmidli, J., 1993. The initial phase of sudden releases of superheated liquid. Doctoral Thesis, No. 10391, Swiss Federal Institute of Technology, Zurich, Switzerland.

Schmidli, J., Yadigaroglu, G., 1995. The sudden release and vaporisation of superheated liquid. In: Heat and Mass Transfer 95, Proceedings of the Second ISHMT – ASME Heat and Mass Transfer Conference and the 13th National Heat and Mass Conference, Surathkal, India, 28–30 December, pp. 349–354.

Shepherd, J.E., Sturtevant, B., 1982. Rapid evaporation at the superheat limit. J. Fluid Mech. 121, 379–402.

Sugioka, I., 1991. Particle transport by rapid vaporization of superheated liquid. Doctoral Thesis, California Institute of Technology, Pasadena, CA, USA.

Yang, Y.-C., Maa, J.R., 1987. Microbubbles in water and boiling superheat. J. Colloid Interface Sci. 120, 87–93.